Chapter 6
Graphene-Based Photocatalysts for the Elimination of Pollutants in Water

Ajay Kumar, Irwing Ramirez, Priyanka Chaudhary, Kuldeep Kumar, Munish Sharma, and Rohit Rana

Abstract Water is an essential part of living things as the life cycle, and water cycle are inextricably linked. The development of industrialization caused the water to become hazardous by emitting dyes, pollutants, organic wastes and other harmful chemicals into the water bodies. It's a big challenge to treat wastewater for human health and to preserve the ecosystem. In recent years, graphene-based photocatalytic materials have gained much attention to eliminate liquid pollutants. This is due to the tremendous optical, electrical and physicochemical properties of this unique two-dimensional material. On integration with other semiconducting, metallic or polymeric materials, graphene remarkably boosts the photocatalytic activity of materials toward contaminants destruction. The high charge carrier mobility, high surface area and excellent mechanical strength of graphene-based nanocomposites make them suitable for photocatalytic applications. This book chapter will focus on the recent significant advances in developing graphene-based photocatalytic materials. The principle of photocatalysis, the basic properties of graphene and the mechanism of how the photocatalytic efficiency against the removal of the liquid pollutant can be enhanced when coupled with graphene has been discussed in this book chapter. Furthermore, current challenges and future recommendations for developing graphene-based photocatalysts are also discussed.

A. Kumar (✉) · I. Ramirez
School of Engineering and Innovation, The Open University, Milton Keynes MK7 6AA, UK
e-mail: ajay.kumar@open.ac.uk

P. Chaudhary
School of Basic Sciences, Advanced Materials Research Center, Indian Institute of Technology Mandi, Kamand, Mandi, Himachal Pradesh 175075, India

K. Kumar · M. Sharma
Department of Physics, School of Basic and Applied Sciences, Maharaja Agrasen University, Solan, Himachal Pradesh 174103, India

R. Rana
Natural Product Chemistry and Process Development Division, CSIR-Institute of Himalayan Bioresource Technology, Palampur, Himachal Pradesh 176061, India

© The Author(s), under exclusive license to Springer Nature Switzerland AG 2023

N. Kumar et al. (eds.), *Two-Dimensional Materials for Environmental Applications*, Springer Series in Materials Science 332, https://doi.org/10.1007/978-3-031-28756-5_6

6.1 Introduction

The demand for fresh water has increased manyfold in the last decade due to increased world's population. According to the report published by United Nations in 2018 on World Water Development, there will be a one-third increase in the demand for drinkable water by 2050 [1]. As clean water is primarily required for various industries and pharmaceutical companies, and households. After use, the release of the water into the environment without treatment adversely affects aquatic as well as human life. Thus, it is highly desirable to treat wastewater using a suitable technique so that it can be reused which can also solve the problem of water scarcity.

To remove the impurities and harmful water pollutants from the waste water, various techniques have been developed with the technological advancements [2]. The waste water can be treated in three effective ways as follows.

(i) Biological treatment,
(ii) Physical treatment, and
(iii) chemical treatment.

Biological treatment of water involves the use of various microbes to degrade the biodegradable water pollutants through biological process. This type of treatment degrade the water pollutant and produce the water, CO_2 and other chemicals. The challenge in this type of water treatment lies in requirement of large area, slow treatment process and bring water to its natural appearance of clean water. Furthermore, physical treatment of water involves physically filter the water using filtration method, sedimentation etc. which again put forward the challenge of slow treating process. It is appreciable in the physical treatment method that no chemicals are used while treating the waste water with physical methods. An another way is chemical method which involves treatment of water through chemical reaction. Oxidation, precipitation, and adsorption are examples of chemical wastewater treatment.

The photocatalytic treatment of wastewater using nanomaterials has gained a lot of attention due to its potential to solve environmental issues, the biggest challenge of the twenty-first century [3, 4]. Many nanomaterials show inherent confinement quantum effects, high surface-to-volume ratio, and large surface area which are favourable to increase the photocatalytic reaction.

Various fundamental issues related to photocatalysts that still need to be resolved before implementing them for large-scale industrial applications. For example, high cost, low efficiency, mismatch of the band gap, recombination of charge carriers and low absorption of solar energy [5]. On absorption of light photons having energy greater than the band gap of the material, the electrons and holes get separated and reside in the conduction band (CB) and valence band (VB), respectively (Fig. 6.1). These separated charge carriers (electrons and holes) migrate towards the surface-active sites wherein they combine with the adsorbed water molecules or moisture to generate highly reactive species such as $OH^{\cdot}$, $O_2^{-\cdot}$, $OOH^{\cdot}$, etc. Further, these highly reactive species react with the pollutant species to mineralize them into CO_2 and water. One could improve the photocatalytic performance of the nanomaterials by addressing the following three key points [6, 7];

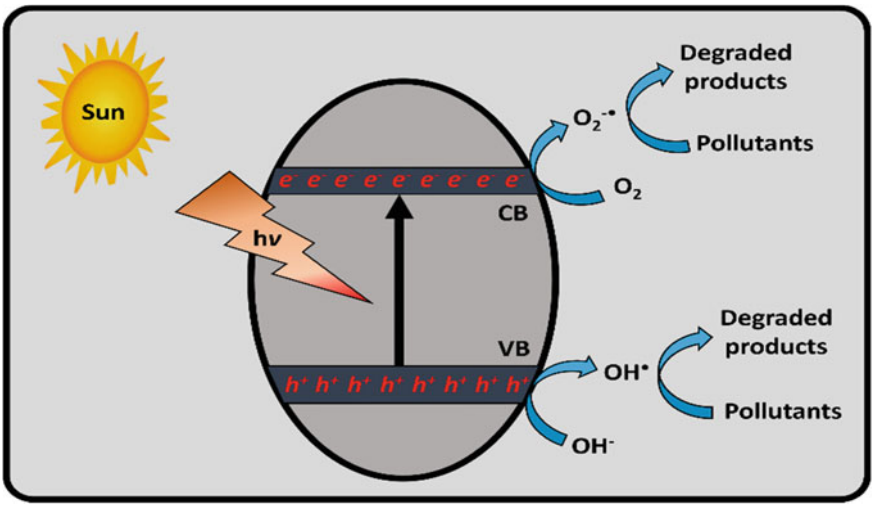

Fig. 6.1 Photoexcitation of the semiconducting materials and subsequent oxidation and reduction reactions for generation of radical species

(1) Absorption of the broad solar spectrum,
(2) Effective separation of the charge carriers, and
(3) Facilitated movement of the separated charge carriers towards the surface-active sites.

Various attempts have been made to improve the efficiency of the photocatalysts such as doping with cationic or anionic species [8], coupling with the metal nanoparticles (NPs) [9] or other semiconductor photocatalysts [10], exfoliation [11] and surface modifications to improve the porosity, surface area, and active facets of the photocatalysts [12, 13]. Despite such modifications at the lab scale, the commercialization of such photocatalytic subsystems for wastewater treatment needs to achieve a certain criterion in terms of cost, efficiency and environmental impact is yet to be realized [14]. Among various two-dimensional support materials, graphene-based materials are the most reliable due to their low cost, high stability and excellent efficiency.

6.2 Basic Properties of Graphene-Based Materials

The carbonaceous materials exhibit unique structural, electrical, and redox properties and tend to add an attractive feature to photocatalysis. The carbonaceous and graphene-based photocatalytic materials have attracted immense attention due to the unique flexible sp^2 hybridized carbon network [15, 16]. Graphene-based materials show promising applications in various fields, such as energy storage [17], biosensors [18], photocatalysis [19], antibacterial and antimicrobial activity [20] etc.

The graphene-based nanomaterials showed excellent electron mobility and electrical conductivity, high optical transparency, and good chemical and thermal stability. Due to the promising electronic and optical properties of graphene-based nanocomposites they are highly demanding in the field of photocatalysis.

Graphene is a two-dimensional layered honeycomb-like structural material formed by sp^2 hybridized carbon atoms. Graphene is a fascinating material with a large surface area, good electrical conductivity, high intrinsic electron mobility and optical transmittance [21, 22]. The two most widely studied derivates of graphene are graphene oxide (GO) and reduced graphene oxide (RGO) [23]. Furthermore, the modified graphene derivatives (graphene, GO and RGO) with other materials such as metals or non-metals or semiconductors, metal–organic frameworks (MOF's) aerogels, etc., offer an outstanding platform for photocatalytic applications. It was found that the modified graphene-based derivative exhibits better photocatalytic and adsorption properties as compared to the pristine graphene [24].

6.3 Synthesis and Properties of Graphene-Based Composites

There are several chemical and physical methods for designing and developing graphene-based composites. Although the chemical vapour deposition and physical exfoliation methods can produce high-quality graphene materials, they show poor dispersion and contact angle due to insufficient functional groups making them less suited for photocatalytic applications [25, 26]. The chemical oxidation of graphene modifies its surface with many oxygen functionalities (hydroxyl, epoxides, carboxyl groups) responsible for increased interlayer distance, thereby allowing better solubility and adsorption of the organic pollutants [26]. In GO, the hydroxyls and epoxides groups are extensively occupied on the basal planes, while the aldehyde, ketone and carboxylic groups are mainly located on the edge of GO [27]. The oxygenated functional groups of GO affect its mechanical, electronic, and electrochemical properties and improve its dispersion in solvents. However, the high dispersion of GO in both aqueous and non-aqueous solvents is challenging during its recovery after the treatment process. Also, the presence of a large number of oxygen functionalities in the GO dimmish its electrical conductivity, which is inappropriate for photocatalytic activity.

To overcome this drawback of GO, further reduction of the oxygen functionalities was made by various techniques. The RGO exhibits similar properties as pristine graphene with restored hexagonal honeycomb-like structure and electrical conductivity due to abundant conjugated π-bonds that were not there in GO [28]. However, with the reduction of oxygen functionalities in RGO, there will be a reduction in the repulsive forces between the sheets, causing lower interlayer distance [29]. The aggregations or restacking due to strong π–π interactions could reduce some potential active sites of RGO nanosheets. However, to prevent the aggregation of RGO

nanosheets various strategies have been used such as surface modification, composite formation, in-situ reduction etc.

Muiva and coworkers prepared multilayered graphene/zinc oxide (MLG/ZnO) nanocomposite using ex-situ casting of ZnO and MLG nanopowders [30]. The MLG wasobtained via a green route from cellulose extracted from corn husk. The extracted cellulose was pyrolyzed at 800 °C for 2 h under a nitrogen atmosphere (Fig. 6.2). The carbonized corn husk (CH-C) was mixed homogeneously with KOH and pyrolyzed again in a nitrogen atmosphere to activate the carbon material (CH-CA). Finally, the activated material was treated with H_2SO_4 to etch out intercalated K^+ ions resulting in highly porous and activated MLG nanosheets. Furthermore, the prepared nanocomposite was used for the photocatalytic degradation of congo red (CR) and rhodamine B (RhB) under natural sunlight irradiations.

Recently, our group has synthesized a ternary nanocomposite of 2D-2D GCN/RGO heterojunction decorated with Au nanostars (NST) using a hydrothermal synthesis route (Fig. 6.3) [31]. A chemical reduction method was used for the synthesis of the Au NST. The mixture of the Au NST, protonated GCN and GO with negative surface charge was treated hydrothermally to synthesize the composite with strong electrostatic interactions. Further, a series of nanocomposites were synthesized by varying the weight ratio as 1, 2, 3, and 5 wt%. It was found that the

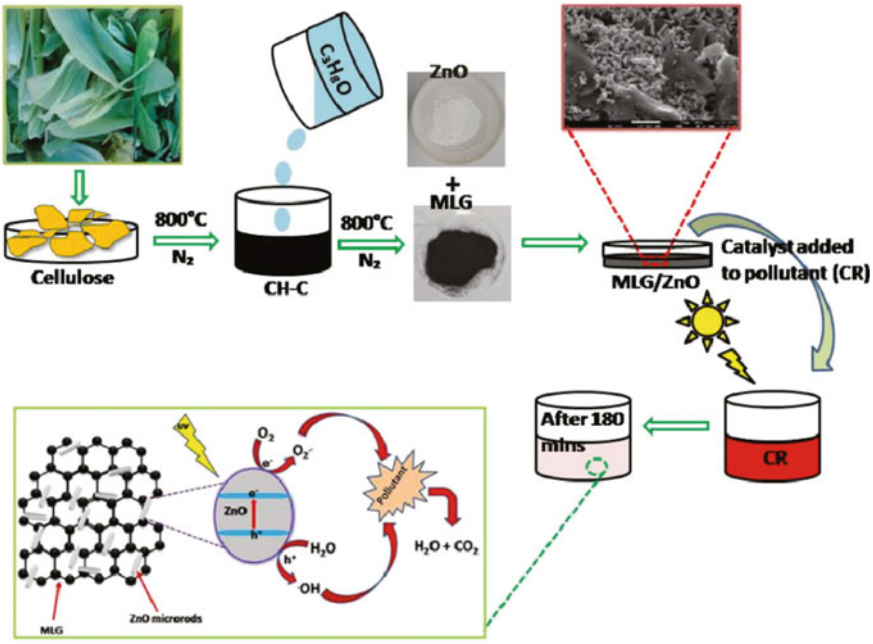

Fig. 6.2 Schematic presentation for the synthesis of multilayered graphene/ZnO nanocomposite and its photocatalytic activity for the degradation of organic pollutants. Reproduced with permission from Ref. [30] Copyright 2022, Elsevier Science Ltd.

optimized catalyst ACG2 showed the highest efficiency for the degradation of the methylene blue (MB) and tetracycline (TC) dyes. Similarly, other ternary nanocomposites synthesized using the hydrothermal synthesis route have been reported in the literature for the degradation of organic pollutants such as RGO/ZnO/MoS_2 and CNT/Zno/MoS_2 [32], Ag_3VO_4/Cu-MOF/RGO [33], $AgFeO_2$-graphene/$Cu_2(BTC)_3$ MOF [34], CdS/RGO/BiOI [35], and GCN/graphene/TiO_2 [36].

Furthermore, another synthesis strategy (chemical reflux method) was adopted for the fabrication of RGO nanocomposite with Fe_3O_4@polypyrrole [37]. The free radical polymerization of the pyrrole monomer using ammonium persulfate as an initiator in an acidic solution of GO, resulted in the formation of polypyrrole/RGO (PPy/RGO) nanohybrid. Further, the chemical reflux method was used for the coating of Fe_3O_4 nanorods onto the PPy/RGO nanohybrid as shown in Fig. 6.4a. The XRD patterns show the presence of the characteristic peaks of GO and further the appearance of a broad peak at 24.5° in the PPy/RGO hybrid indicated the successful reduction of GO into RGO (Fig. 6.4b). Similarly, the change in the intensity ratio of D-band due to the defect-filled nature of graphitic carbon at 1347 cm^{-1} and G-band due to

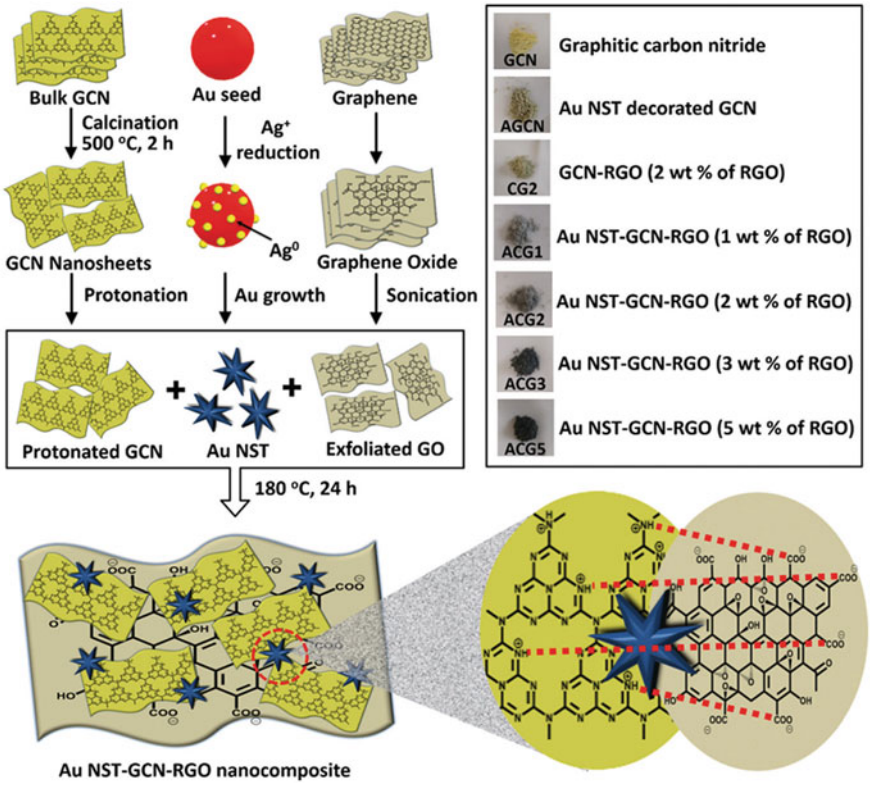

Fig. 6.3 Schematic representation for the synthesis of Au NST/GCN/RGO nanocomposites. Reproduced with permission from Ref. [31]. Copyright 2021, Royal Society of Chemistry

stretching vibration modes in graphitic carbon sheet at 1582 cm^{-1} in Raman spectra indicate a reduction of GO into RGO as shown in Fig. 6.4c. The downward shift of the D and G bands in the representative nanocomposite, Fe_3O_4@PPy/RGO signifies the strong interactions between Fe_3O_4 and PPy/RGO hybrids.

In another report, a quaternary nanocomposite consisting of $NaYF_4$:Yb/Er@CdS core—shell nanostructures decorated with Au NPs supported on RGO nanosheets has been synthesized using the multistep hydrothermal method for the removal of the pharmaceutical pollutant, ciprofloxacin (CIP) [9]. The rational design and development of the catalyst showed the efficient absorption of the broadband solar spectrum (visible and NIR regions). The carbonaceous 2D material, RGO, not only acts as the support for the NPs but plays multiple roles, such as electron acceptor and transporter. In addition, the RGO nanosheet adsorbs the pollutant molecules onto the

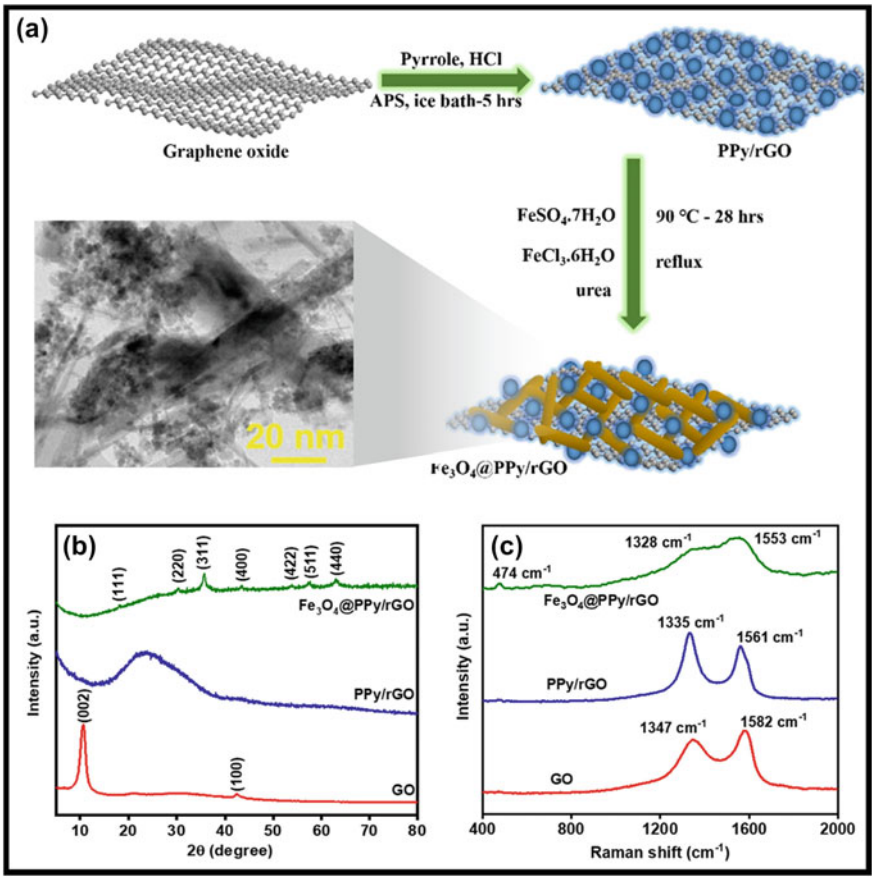

Fig. 6.4 **a** Schematic presentation of the synthesis of Fe_3O_4@PPy/RGO nanocomposite, **b** XRD patterns and **c** Raman spectra of GO, PPy/RGO and Fe_3O_4@PPy/RGO nanocomposite. Reproduced with permission from Ref. [37]. Copyright 2021, Elsevier Science Ltd.

surface, thereby facilitating their photocatalytic degradation. Other quaternary photocatalytic materials are also reported in the literature for the removal of the organic and inorganic contaminants from the wastewater, for example, Ag_2CrO_4/TiO_2/Au/RGO hybrid biofilm [38], Carbon QDs/RGO-S@GCN/B@GCN [39], etc.

6.4 Photocatalytic Degradation of Organic Pollutants

Various intermediates and radical species are generated after photoexciting the graphene-based photocatalysts. These species are responsible for destroying both organic and inorganic components of pollutants in wastewater. Table 6.1 summarizes the recent reports on the photocatalytic degradation of organic pollutants using graphene-based nanocomposites. Peng et al., have synthesized 2D-2D GCN/GO nanocomposite using a hydrothermal synthesis route through π-π stacking interactions [40]. Further, the Ag NPs were uniformly deposited onto GCN/GO nanocomposite through the *in-situ* reduction method. As-synthesized nanocomposite was used for surface-enhanced Raman scattering (SERS) detection of biomolecules (adenine) and adsorption and photocatalytic degradation of organic pollutants (methylene blue).

A TiO_2/GO nanocomposite synthesized using the hydrothermal method was used to treat mineral processing wastewater photocatalytically [41]. The UV–Vis diffuse reflectance spectroscopy (DRS) analysis showedan extraordinary improvement in the absorption of the TiO_2 in the visible region after loading 18% of GO (Fig. 6.5a). Furthermore, the photocurrent measurements showed the higher photocurrent density of the 18% TiO_2/G nanocomposite as compared to the bare graphene nanosheets indicating the efficient separation of the charge carriers for better photocatalytic performance (Fig. 6.5b). The representative nanocomposite showed a degradation efficiency of 97.03% in 190 min under visible light irradiations (Fig. 6.5c). The improved photocatalytic performance of the catalyst was attributed to the huge specific surface area, low electron–hole suppression rate and extended absorption in the visible range. The bare GO shows a high rate of removal of the dye for an initial 30 min that could possibly be due to the adsorption process. However, the removal rate decreases significantly with further increases in time. Figure 6.5d depicts the EPR spectra suggesting that the higher intensity in 18% TiO_2/G nanocomposite under visible light irradiations is due to high oxygen vacancies in the samples. The EPR analysis showed that the 18% TiO_2/G photocatalytic material can be easily excited under visible light to generate electrons responsible for its high photocatalytic performance.

In another report, Graphene-based ZnCr layered double hydroxide (LDH) nanocomposites were utilized for the sonophotocatalytic performances for the degradation of rifampicin dye [42]. For this purpose, the ZnCr LDH and its nanocomposite with RGO were synthesized using a facile co-precipitation method., The maximum degradation efficiency of 87.3%, was achieved for rifampicin dye within 60 min of visible light irradiation. The high photocatalytic performance of the ZnCr

Table 6.1 Summary of graphene-based photocatalysts for degradation of pollutants in wastewater

Photocatalysts	Light source	Pollutants concentration	Reaction time	Year (Ref.)
Ag NPs/GCN/GO nanocomposite	Visible light (405 nm)	RhB (1×10^{-6} M)	60 min	(2022) [40]
Corn husk multi-layered graphene/ZnO nanocomposite	Natural sunlight	RhB, CR and DOX (1.25×10^{-5} mol L^{-1})	RhB (86%), CR (100%) and DOX (90%) in 180 min	(2022) [30]
Indium hydroxide/Nitrogen-doped graphene aerogels	High-pressure mercury lamp (400 W)	*p*-NP (20 mg L^{-1})	98% in 180 min	(2022) [44]
B doped RGO supported bismuth ferrite	300 W Xenon lamp	TC and RhB (10 mg L^{-1})	TC (86.7%) and RhB (99.4%) in 90 min	(2022) [45]
RGO-TiO_2 (photocatalysis linked with Fenton process)	shortwave light (UV254), black light (UV365), UV LED torch (UV395), visible light (400–700 nm) and sunlight	PA (200 mg L^{-1})	100% in 24 min (UV254), 22 min (UV365), 19 min (UV395), 18 min (VIS), 15 min (sunlight)	(2022) [46]
3D graphene/$Cd_{0.5}Zn_{0.5}S$ hybrids	300 W Xenon lamp ($\lambda >$ 420 nm)	CIP (5 mg L^{-1})	95% removal in 15 min	(2022) [47]
ZnCr LDH/RGO nanocomposite	LED lamp (visible light)	RIF (15 mg L^{-1})	87.3% removal in 60 min	(2022) [42]
TiO_2/graphene nanocomposite	300 W Xenon lamp	PBX (20 mg L^{-1})	97.03% in 130 min	(2022) [41]
Graphene- AgNPs@GCN	Visible light	MB (5 mg L^{-1})	88.5% in 140 min	(2022) [48]
$FeTiO_3$/GO nanocomposite	150 W Xenon lamp	Phenol (50 mg L^{-1})	100% in 150 min	(2021) [49]
$ZnSnO_3$/graphene aerogel	Simulated sunlight	CIP (100 mg L^{-1})	100% in 120 min	(2021) [43]
Fe_3O_4 NRs-polypyrrole/RGO	Two 250 W tungsten-halogen lamps	ACP (1 mg L^{-1})	84% in 120 min	(2021) [37]

(continued)

Table 6.1 (continued)

Photocatalysts	Light source	Pollutants concentration	Reaction time	Year (Ref.)
RGO/Zno/MoS_2 ternary nanocomposite	Visible light (100 W)	Aniline (80 mg L^{-1})	100% in 120 min	(2020) [32]
RGO-Bi_2WO_6	85 W CFL bulbs (450–650 nm)	LVX (80 mg L^{-1})	74.3% in 120 min	(2020) [50]
Ag_3VO_4/Cu-MOF/RGO	Visible light	AB92 (10 mg L^{-1})	80% in 120 min	(2020) [33]
$AgFeO_2$-graphene/$Cu_2(BTC)_3$ MOF	Natural sunlight	AMC and DCF (5 mg L^{-1})	AMC (92.9%) and DCF (91.4%) in 150 min	(2020) [34]
Carbon QDs/RGO-S@GCN/B@GCN	300 W Xe lamp (450 mW cm^{-2}, 380–780 nm) and direct sunlight	CMP (10 mg L^{-1})	Visible light 90% in 120 min) and sunlight (99.2% in 90 min)	(2020) [39]
Ag_2CrO_4/TiO_2/Au/RGO biofilm	125 W Hg lamp	MB (10 mg L^{-1})	97% in 52 min	(2020) [38]
RGO-N-ZnO	500 W tungsten halogen lamp	MB (10 mg L^{-1})	98.5% in 120 min	(2020) [51]
GO/TiO_2	500 W Xenon lamp	MB (5 mg L^{-1})	92% in 60 min	(2020) [52]
N doped graphene/TiO_2	300 W mercury lamp	BPA (20 mg L^{-1})	100% in 60 min	(2020) [53]
GO-derived C-doped $SrTiO_3$	500 W Xenon lamp	MB (8 mg L^{-1}), MO (3.3 mg L^{-1}), RhB (4.8 mg L^{-1}), phenol (9.4 mg L^{-1})	Over 95% of MO, MB, and RhB, and 70% of phenol and BPA in 3 h	(2020) [54]
Lanthanum-substituted Zn spinel ferrite @RGO	UV lamp (0.6 mW cm^{-2})	RhB (30 mg L^{-1})	100% in 60 min	(2020) [55]
GCN/graphene/TiO_2	300 W Xenon lamp (300 mW cm^{-2})	TC (15 mg L^{-1}), CIP (3 mg L^{-1}), BPA (5 mg L^{-1}) and RhB (20 mg L^{-1})	TC (83.5%) in 80 min, CIP (61.7%) in 60 min, BPA (79.5%) in 70 min and RhB (98.0%) in 50 min	(2020) [36]

(continued)

Table 6.1 (continued)

Photocatalysts	Light source	Pollutants concentration	Reaction time	Year (Ref.)
Bi_2S_3-$BiVO_4$ graphene aerogel	300 W Xe lamp ($\lambda > 420$ nm)	Cr (VI) (50 mg L^{-1}) and BPA (10 mg L^{-1})	99% removal of Cr (VI) and BPA in 120 min	(2020) [56]
GO/ZnO-Ag nanocomposite	Natural sunlight	MB (3.13×10^{-5} M)	100% in 40 min using GO/ZnO-Ag	(2020) [57]
CuO-TiO_2/RGO	UV light (312 nm)	MO (10 mg L^{-1})	99% in 90 min	(2019) [58]
SnO_2 aerogel/rGO nanocomposite	40 W UV lamp (370 nm)	MO (1×10^{-5} M)	84% in 60 min	(2019) [59]
GO/TiO_2	Hg lamp	RhB (10 mg L^{-1}) and AG25 (40 mg L^{-1})	100% in 120 min (RhB) and 97% in 180 min (AG25)	(2019) [60]
Graphene based NiAlFe LDH	500 W Xe lamp	CIP (10 mg L^{-1})	93% in 120 min	(2019) [61]
SnS_2/RGO	65 W CFL lamp ($\lambda > 400$ nm)	RBB and RBR (10 ppm)	99.7% (RBB) and 97% (RBR) in 150 min	(2019) [62]
Porous graphene/ZnO	Natural sunlight	MO (13 mg L^{-1})	100% in 150 min	(2019) [63]
CdS/RGO/BiOI	500 W Xe lamp ($\lambda > 420$ nm)	MDHB (20 mg L^{-1})	~80% in 240 min	(2019) [35]
Ordered Porous TiO_2-Pt/RGO	300 W Xe lamp ($\lambda > 420$ nm)	MO (20 mg L^{-1})	82% in 120 min	(2019) [64]
RGO-ZnTe	Solar simulator	TC (10 mg L^{-1})	~70% in 45 min	(2019) [65]

AB92 = acid blue 92; ACP = acetaminophen; AG25 = acid green 25; AMC = amoxicillin; BPA = bisphenol A; CMP = Chloramphenicol; CIP = ciprofloxacin; CR = congored; DCF = diclofenac; DOX = doxycycline; GCN = graphitic carbon nitride; GO = graphene oxide; LDH = layered double hydroxide; LVX = levofloxacin; MB = methylene blue; MDBH = methyl 3,5-dichloro-4-hydroxybenzoate; MO = methyl orange; NPs = nanoparticles; *p*-NP = p-nitrophenol; PA = picric acid; PBX = potassium butyl xanthate;RBB = remazol brilliant blue; RBR = remazol brilliant red; RGO = reduced graphene oxide; RhB = rhodamine B; RIF = rifampicin; TC = tetracycline

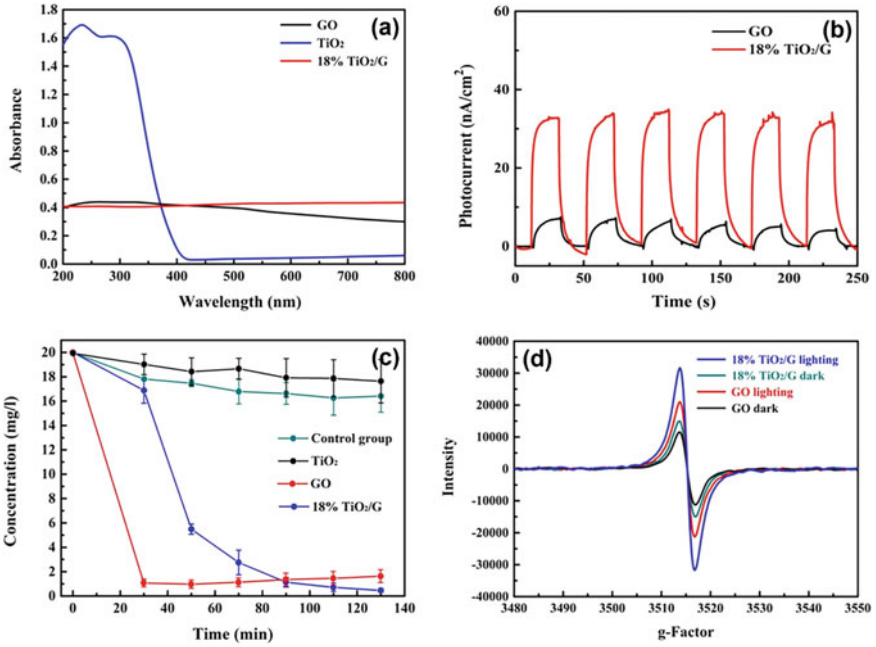

Fig. 6.5 **a** UV–VIS-DRS spectra, **b** photocurrent-time (I-t) plot, **c** photocatalytic activity under visible light and **d** EPR spectra of GO and 18% TiO_2/G nanocomposite. Reproduced with permission from Ref. [41] Copyright 2022, Elsevier Science Ltd.

LDH/RGO nanocomposite was attributed to the enhancement in the production of active hydroxyl ($OH^{\cdot}$) radical species under visible light irradiations. The radical scavenger studies confirm that the $OH^{\cdot}$ radical plays the most significant role in degrading the dye molecule. Furthermore, the ultrasonication process benefits the process by preventing the agglomeration of the catalyst in solution, improving mass transport and increasing the availability of the active sites by continuously cleaning of the catalyst surface.

A macroscopic $ZnSnO_3$/graphene aerogel structure has been synthesized that showed excellent adsorption and degradation of the CIP from wastewater under visible light irradiations [43]. The catalyst synthesized with an optimized mass ratio (1:2) of the $ZnSn(OH)_6$ to GO, denoted as ZGA-4, exhibits the 100% removal efficiency of the pollutant. The improved photocatalytic performance of the catalyst was ascribed to the optimized interfacial and electronic band structures responsible for the separated photogenerated charge carriers and immensely produced active species such as $OH^{\cdot}$ and $O_2^{-\cdot}$ radicals, as shown in Fig. 6.6.

The graphene-based materials play a major role in enhancing the photocatalytic activity of the semiconducting materials for the degradation of organic pollutants. Various intermediates and radical species are generated after photoexciting the graphene-based photocatalysts. These species are responsible for destroying both

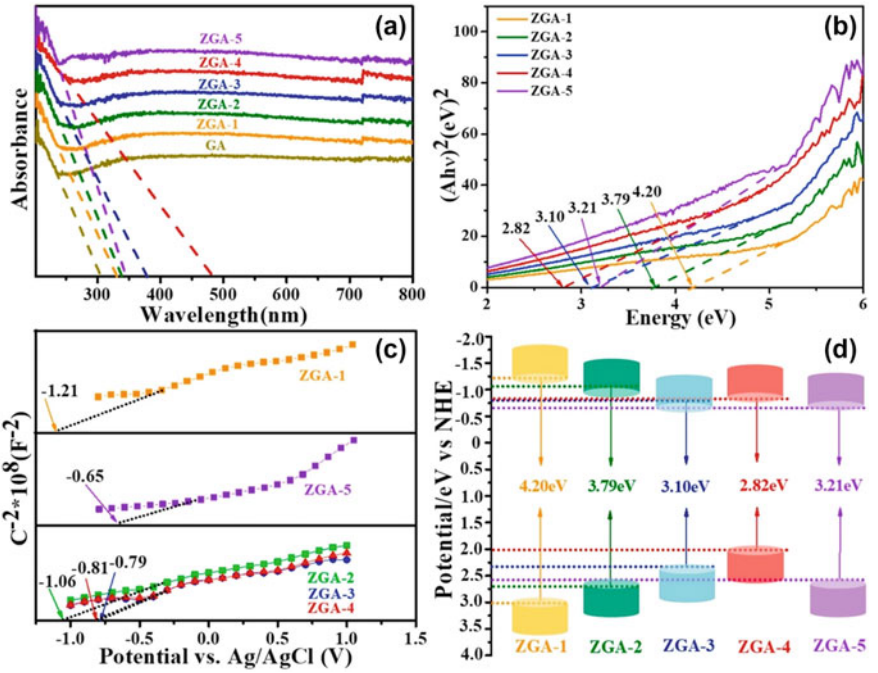

Fig. 6.6 **a** UV–VIS diffuse reflectance spectra; **b** Tauc's plots; **c** Mott-Schottky diagram and **d** band gaps of the ZGA nanocomposites. Reproduced with permission from Ref. [43] Copyright 2021, Elsevier Science Ltd.

organic and inorganic components of pollutants in wastewater. Table 6.1 summarizes the recent reports on the photocatalytic degradation of organic pollutants using graphene-based nanocomposites.

6.5 Summary and Future Perspective

In summary, graphene-based materials open new opportunities in the advanced photocatalysis process. The outstanding physical and chemical properties of graphene-based photocatalysts such as large surface area, high electron conductivity, abundant surface-active sites, high mechanical strength and good adsorption and reusability properties make it the most reliable candidate in the field of photocatalysis. This chapter discusses various strategies, such as surface modification, doping, and multijunction formation, to improve the photocatalytic performance of graphene-based materials. Coupling the two-dimensional carbonaceous materials (graphene, GO and RGO) with other nanomaterials like metal oxides and metal nanoparticles exhibit synergistic improvement in the photocatalytic efficiency and stability of the catalyst. Also, the optimized amount of graphene-based materials in

the catalyst tunes the bandgap to enhance the light absorption of the catalyst. From the above discussion of the literature on binary, ternary, and quaternary composites of graphene-based materials, it can be concluded that the appropriate modification could result from highly efficient materials for adsorption and photocatalytic treatment of wastewater. The production of cost-effective, photostable and efficient graphene-based materials at a large scale is most desirable and challenging as well. Thus, more work needs to be done by researchers to ensure the commercialization of such materials for large-scale photocatalytic applications. There are extensive opportunities in the research area to extend the perspective of graphene-based materials for wastewater treatment.

Acknowledgements Ajay Kumar and Irwing Ramirez acknowledge Waste2Fresh grant under Horizon 2020 program. The authors thank The Open University for granting financial resources, access to facilities, and training to conduct this work.

References

1. U. Water, *2018 UN World Water Development Report, Nature-based Solutions for Water* (2018)
2. A. Saravanan et al., Effective water/wastewater treatment methodologies for toxic pollutants removal: processes and applications towards sustainable development. Chemosphere **280**, 130595 (2021)
3. F.E. Osterloh, Inorganic materials as catalysts for photochemical splitting of water. Chem. Mater. **20**(1), 35–54 (2008)
4. S. Jamaly, A. Giwa, S.W. Hasan, Recent improvements in oily wastewater treatment: progress, challenges, and future opportunities. J. Environ. Sci. **37**, 15–30 (2015)
5. S.M. Gupta, M. Tripathi, A review of TiO_2 nanoparticles. Chinese Sci. Bull. **56**(16), 1639–1657
6. C. Belver et al., Semiconductor Photocatalysis for Water Purification, in *Nanoscale Materials in Water Purification.* (Elsevier, 2019), pp.581–651
7. Y. Xu et al., Rate enhancement and rate inhibition of phenol degradation over irradiated anatase and rutile TiO_2 on the addition of NaF: new insight into the mechanism. J. Phys. Chem. C **111**(51), 19024–19032 (2007)
8. A. Kudo et al., Effects of doping of metal cations on morphology, activity, and visible light response of photocatalysts. Chem. Phys. **339**(1–3), 104–110 (2007)
9. A. Kumar et al., Rational design and development of lanthanide-doped $NaYF_4$@ CdS–Au–RGO as quaternary plasmonic photocatalysts for harnessing visible–near-infrared broadband spectrum. ACS Appl. Mater. Interf. **10**(18), 15565–15581 (2018)
10. R. Marschall, Semiconductor composites: strategies for enhancing charge carrier separation to improve photocatalytic activity. Adv. Func. Mater. **24**(17), 2421–2440 (2014)
11. P. Qiu et al., Fabrication of an exfoliated graphitic carbon nitride as a highly active visible light photocatalyst. J. Mater. Chem. A **3**(48), 24237–24244 (2015)
12. H. Park et al., Surface modification of TiO_2 photocatalyst for environmental applications. J. Photochem. Photobiol., C **15**, 1–20 (2013)
13. M. Li et al., Facet, junction and electric field engineering of bismuth-based materials for photocatalysis. ChemCatChem **10**(20), 4477–4496 (2018)
14. M. Kitano et al., Recent developments in titanium oxide-based photocatalysts. Appl. Catal. A **325**(1), 1–14 (2007)
15. T. Wehling et al., Molecular doping of graphene. Nano Lett. **8**(1), 173–177 (2008)

16. P.V. Kamat, Graphene-based nanoassemblies for energy conversion. J. Phys. Chem. Lett. **2**(3), 242–251 (2011)
17. R. Kumar, et al., Laser processing of graphene and related materials for energy storage: state of the art and future prospects. Progr. Energy Combust. Sci. 100981 (2022)
18. C. Deepa, L. Rajeshkumar, M. Ramesh, Preparation, synthesis, properties and characterization of graphene-based 2D nano-materials for biosensors and bioelectronics. J. Mater. Res. Technol. (2022)
19. M. Sajna, et al., An overview of graphene-based 2D/3D nanostructures for photocatalytic applications. Top. Catal. 1–25 (2022)
20. G. Lekshmi et al., Multifunctional oil-produced reduced graphene oxide–silver oxide composites with photocatalytic, antioxidant, and antibacterial activities. J. Colloid Interf. Sci. **608**, 294–305 (2022)
21. S. Guo, S. Dong, Graphene nanosheet: synthesis, molecular engineering, thin film, hybrids, and energy and analytical applications. Chem. Soc. Rev. **40**(5), 2644–2672 (2011)
22. C. Zhu, D. Du, Y. Lin, Graphene and graphene-like 2D materials for optical biosensing and bioimaging: a review. 2D Mater. **2**(3), 032004 (2015)
23. Y. Ai et al., Insights into the adsorption mechanism and dynamic behavior of tetracycline antibiotics on reduced graphene oxide (RGO) and graphene oxide (GO) materials. Environ. Sci. Nano **6**(11), 3336–3348 (2019)
24. A. Gulati, R. Kakkar, Graphene-based adsorbents for water remediation by removal of organic pollutants: theoretical and experimental insights. Chem. Eng. Res. Des. **153**, 21–36 (2020)
25. X. Cui et al., Liquid-phase exfoliation, functionalization and applications of graphene. Nanoscale **3**(5), 2118–2126 (2011)
26. H.M. Hegab, L. Zou, Graphene oxide-assisted membranes: fabrication and potential applications in desalination and water purification. J. Membr. Sci. **484**, 95–106 (2015)
27. X.J. Lee et al., Review on graphene and its derivatives: synthesis methods and potential industrial implementation. J. Taiwan Inst. Chem. Eng. **98**, 163–180 (2019)
28. S. Gupta et al., Emerging trends in the syntheses of heterocycles using graphene-based carbocatalysts: an update. Top. Curr. Chem. **377**(3), 1–62 (2019)
29. C.M. Park et al., Potential utility of graphene-based nano spinel ferrites as adsorbent and photocatalyst for removing organic/inorganic contaminants from aqueous solutions: a mini review. Chemosphere **221**, 392–402 (2019)
30. D.P. Sebuso et al., Corn husk multilayered graphene/ZnO nanocomposite materials with enhanced photocatalytic activity for organic dyes and doxycycline degradation. Mater. Res. Bull. **151**, 111800 (2022)
31. A. Kumar et al., Plasmon induced hot electron generation in two dimensional carbonaceous nanosheets decorated with Au nanostars: enhanced photocatalytic activity under visible light. Mater. Chem. Front. **5**(3), 1448–1467 (2021)
32. P. Ghasemipour et al., Developing the ternary ZnO doped MoS_2 nanostructures grafted on CNT and reduced graphene oxide (RGO) for photocatalytic degradation of aniline. Sci. Rep. **10**(1), 1–16 (2020)
33. E. Akbarzadeh et al., Preparation and characterization of novel Ag_3VO_4/Cu-MOF/rGO heterojunction for photocatalytic degradation of organic pollutants. Mater. Res. Bull. **121**, 110621 (2020)
34. E.M. El-Fawal, S.A. Younis, T. Zaki, Designing $AgFeO_2$-graphene/Cu_2 $(BTC)_3$ MOF heterojunction photocatalysts for enhanced treatment of pharmaceutical wastewater under sunlight. J. Photochem. Photobiol. A: Chem. **401**, 112746 (2020)
35. N. Ma et al., In situ synthesis of a cadmium sulfide/reduced graphene oxide/bismuth Z-scheme oxyiodide system for enhanced photocatalytic performance in chlorinated paraben degradation. Chem. Eng. J. **359**, 530–541 (2019)
36. Z. Wu et al., MXene Ti_3C_2 derived Z–scheme photocatalyst of graphene layers anchored TiO_2/g–C_3N_4 for visible light photocatalytic degradation of refractory organic pollutants. Chem. Eng. J. **394**, 124921 (2020)

37. R.S. Kumar et al., Fe_3O_4 nanorods decorated on polypyrrole/reduced graphene oxide for electrochemical detection of dopamine and photocatalytic degradation of acetaminophen. Appl. Surf. Sci. **556**, 149765 (2021)
38. R. Biswas et al., Novel green approach for fabrication of Ag_2CrO_4/TiO_2/Au/r-GO hybrid biofilm for visible light-driven photocatalytic performance. J. Phys. Chem. C **124**(5), 3373–3388 (2020)
39. A. Kumar et al., Carbon quantum dots and reduced graphene oxide modified self-assembled $S@C_3N_4/B@C_3N_4$ metal-free nano-photocatalyst for high performance degradation of chloramphenicol. J. Mol. Liq. **300**, 112356 (2020)
40. G.-Z. Peng et al., Photocatalytic degradation and reusable SERS detection by Ag nanoparticles immobilized on g-C_3N_4/graphene oxide nanosheets. Surf. Coat. Technol. **435**, 128212 (2022)
41. M. Jiang et al., Photocatalytic degradation of xanthate in flotation plant tailings by TiO_2/graphene nanocomposites. Chem. Eng. J. **431**, 134104 (2022)
42. T.S. Rad et al., Graphene-based ZnCr layered double hydroxide nanocomposites as bactericidal agents with high sonophotocatalytic performances for degradation of rifampicin. Chemosphere **286**, 131740 (2022)
43. S. Dong et al., Interfacial and electronic band structure optimization for the adsorption and visible-light photocatalytic activity of macroscopic $ZnSnO_3$/graphene aerogel. Compos. B Eng. **215**, 108765 (2021)
44. Y. Jiang, J. Zhang, R. Balasubramanian, Nitrogen-doped graphene aerogels with rational indium hydroxide decoration for highly efficient photocatalytic of p-nitrophenol. J. Environ. Chem. Eng. **10**(1), 107125 (2022)
45. R. Preetha et al., Promoting photocatalytic interaction of boron doped reduced graphene oxide supported $BiFeO_3$ nanocomposite for visible-light-induced organic pollutant degradation. J. Alloy. Compd. **904**, 164038 (2022)
46. B. Usharani, V. Manivannan, Enhanced photocatalytic activity of reduced graphene oxide-TiO_2 nanocomposite for picric acid degradation. Inorg. Chem. Commun. **142**, 109660 (2022)
47. G. Zeng et al., Highly efficient photocatalytic degradation of the emerging pollutant ciprofloxacin via the rational design of a magnetic interfacial junction of mangosteen peel waste-derived 3D graphene hybrid material. Environ. Sci. Nano **9**(4), 1298–1314 (2022)
48. C. Chen et al., Graphene nanofiltration membrane intercalated with AgNP@g-C_3N_4 for efficient water purification and photocatalytic self-cleaning performance. Chem. Eng. J. **441**, 136089 (2022)
49. M. Moradi et al., Ultrasound-assisted synthesis of $FeTiO_3$/GO nanocomposite for photocatalytic degradation of phenol under visible light irradiation. Sep. Purif. Technol. **261**, 118274 (2021)
50. M. Arya et al., Hydrothermal synthesis of rGO-Bi_2WO_6 heterostructure for the photocatalytic degradation of levofloxacin. Opt. Mater. **107**, 110126 (2020)
51. M. Suresh, A. Sivasamy, Fabrication of graphene nanosheets decorated by nitrogen-doped ZnO nanoparticles with enhanced visible photocatalytic activity for the degradation of Methylene Blue dye. J. Mol. Liq. **317**, 114112 (2020)
52. T.A. Kurniawan et al., Functionalizing TiO_2 with graphene oxide for enhancing photocatalytic degradation of methylene blue (MB) in contaminated wastewater. J. Environ. Manage. **270**, 110871 (2020)
53. Y. Zhao et al., Enhanced activation of peroxymonosulfate by nitrogen-doped graphene/TiO_2 under photo-assistance for organic pollutants degradation: Insight into N doping mechanism. Chemosphere **244**, 125526 (2020)
54. C.-W. Chang, C. Hu, Graphene oxide-derived carbon-doped $SrTiO_3$ for highly efficient photocatalytic degradation of organic pollutants under visible light irradiation. Chem. Eng. J. **383**, 123116 (2020)
55. B.-M. Jun et al., Accelerated photocatalytic degradation of organic pollutants over carbonate-rich lanthanum-substituted zinc spinel ferrite assembled reduced graphene oxide by ultraviolet (UV)-activated persulfate. Chem. Eng. J. **393**, 124733 (2020)

56. Q. Liang et al., Simultaneous Cr (VI) reduction and bisphenol A degradation by a 3D Z-scheme Bi_2S_3-$BiVO_4$ graphene aerogel under visible light. Chem. Eng. J. **384**, 123256 (2020)
57. N.A. Al-Rawashdeh, O. Allabadi, M.T. Aljarrah, Photocatalytic activity of graphene oxide/zinc oxide nanocomposites with embedded metal nanoparticles for the degradation of organic dyes. ACS Omega **5**(43), 28046–28055 (2020)
58. S.G. Babu et al., Synergistic effect of sono-photocatalytic process for the degradation of organic pollutants using CuO–TiO_2/rGO. Ultrason. Sonochem. **50**, 218–223 (2019)
59. T. Kim et al., Facile synthesis of SnO_2 aerogel/reduced graphene oxide nanocomposites via in situ annealing for the photocatalytic degradation of methyl orange. Nanomaterials **9**(3), 358 (2019)
60. M. Adly, S.M. El-Dafrawy, S. El-Hakam, Application of nanostructured graphene oxide/titanium dioxide composites for photocatalytic degradation of rhodamine B and acid green 25 dyes. J. Mater. Res. Technol. **8**(6), 5610–5622 (2019)
61. J. Liang et al., Constructing high-efficiency photocatalyst for degrading ciprofloxacin: three-dimensional visible light driven graphene based NiAlFe LDH. J. Colloid Interf. Sci. **540**, 237–246 (2019)
62. L. Dashairya et al., SnS_2/RGO based nanocomposite for efficient photocatalytic degradation of toxic industrial dyes under visible-light irradiation. J. Alloy. Compd. **774**, 625–636 (2019)
63. L. Wang et al., Enhanced photocatalytic degradation of methyl orange by porous graphene/ZnO nanocomposite. Environ. Pollut. **249**, 801–811 (2019)
64. J. Huo, C. Yuan, Y. Wang, Nanocomposites of three-dimensionally ordered porous TiO_2 decorated with Pt and reduced graphene oxide for the visible-light photocatalytic degradation of waterborne pollutants. ACS Appl. Nano Mater. **2**(5), 2713–2724 (2019)
65. K. Chakraborty, T. Pal, S. Ghosh, RGO-ZnTe: a graphene based composite for tetracycline degradation and their synergistic effect. ACS ACS Appl. Nano Mater. **1**(7), 3137–3144 (2018)